Journal of Inorganic and Organometallic Polymers and Materials (2018) 28:1114–1126
https://doi.org/10.1007/s10904-017-0772-9

Influence of TiO_2 Incorporation on the Microstructure, Optical, and Dielectric Properties of TiO_2/Epoxy Composites

A. Bouzidi[1,2] · K. Omri[3] · W. Jilani[1,4] · H. Guermazi[1] · I. S. Yahia[5,6,7]

Received: 29 October 2017 / Accepted: 18 December 2017 / Published online: 26 December 2017

Abstract
This study begins with a synthesis and characterization of Epoxy/TiO_2 composites (Ep–TiO_2–Cs) with different TiO_2 fillers. The ultrasonic mixing process was employed to disperse the TiO_2 fillers into the epoxy resin matrix. The effect of TiO_2 contents on microstructural, optical and electrical properties of the Ep–TiO_2–Cs have investigated. Several techniques are now being used to characterize the Ep–TiO_2–Cs. The microstructure of fracture surfaces was examined by SEM techniques. It revealed that the as-prepared TiO_2 particles are a spherical shape structure. At 5.0 wt% TiO_2 fillers, it is evident that these spheres are homogeneously distributed in the epoxy matrix. The XRD study confirms that the particle size generally decreases with increasing the added TiO_2 fillers in the epoxy matrix. In the UV-light range, the neat epoxy only blocks UV-light in the range of 200–280 nm, it becomes high UV-light blocker (up to 400 nm) via the addition of TiO_2 powder with 5.0 wt% fillers. Moreover, the TiO_2 content addition obviously enhanced the UV-Shielding efficiency of the epoxy resin.

Keywords Composites · Microstructure · TiO_2 · Optical properties · Dielectric properties

1 Introduction

For power engineering, organic–inorganic material composites represent not only a new and exciting field of basic research, but also offers perspectives for several new applications in different technological fields due to their low cost, good processability, high transparency in the visible range, broad and interdisciplinary area of fundamental research and development activity [1, 2]. In general, nanoparticles were introduced into polymer matrix using various techniques. The various dispersion processes are necessary in order to transfer the nanoparticles from the agglomerated state into a homogeneously dispersed state. The direct incorporation using chemical methods and by application of high shear forces during mechanical powder dispersion process are the popular one [3–5]. Ultrasound vibration was used to disperse nanoparticles, which also helps to improve the dispersion state of nanoparticles. Chemical methods are able to generate individual and non-agglomerated nanoparticles "in situ" within a thermosetting/thermoplastic polymer. However, an additional chemical treatment of the nanoparticle surface

✉ A. Bouzidi
abdelfatteh.bouzidi@yahoo.fr

✉ K. Omri
omrikarim16@gmail.com

[1] Research Unit, Physics of Insulating and Semi Insulating Materials, Faculty of Sciences, University of Sfax, B.P. 1171, 3000 Sfax, Tunisia

[2] Technical and Vocational Training Corporation: Technical College Branch, P.O.B 10, 61974 Ahad Rufidah, Kingdom of Saudi Arabia

[3] Laboratoire de Physique des Matériaux et des Nanomatériaux Appliquée à l'Environnement, Faculté des Sciences de Gabès, Cité Erriadh Manara Zrig, 6072 Gabès, Tunisia

[4] Department of Physics, Faculty of Science Sciences and Arts Dhahran Al Janoub, King Khalid University, P.O. Box 960, 61421 Abha, Kingdom of Saudi Arabia

[5] Research Center for Advanced Materials Science (RCAMS), King Khalid University, P.O. Box 9004, 61413 Abha, Kingdom of Saudi Arabia

[6] Advanced Functional Materials & Optoelectronic Laboratory (AFMOL), Department of Physics, Faculty of Science, King Khalid University, P.O. Box 9004, Abha, Kingdom of Saudi Arabia

[7] Nanoscience Laboratory for Environmental and Bio-medical Applications (NLEBA), Semiconductor Lab., Department of Physics, Faculty of Education, Ain Shams University, Roxy, 11757 Cairo, Egypt

may further enhance the composite's properties by improving the filler-matrix coupling quality [3–5].

TiO_2 is an amorphous white powder and it is a very stable material. The TiO_2 material is produced and used in the workplace in varying particle size contents, including fine and ultrafine sizes. Therefore, it is used extensively and finding applications in several commercial products such as cosmetics, plastics, paper and food. Therefore, TiO_2 nanospheres have been considered biologically inactive in experimental animals [6] and humans [7]. The TiO_2 nanoparticles have been proposed as one of the promising candidates to achieve high refractive index and maintain high transparency, because it have a high refractive index (n = 2.45 and 2.7 for anatase and rutile phase, respectively) and a very low absorption coefficient in the visible range [8]. In the frame of environmental protection, TiO_2 becomes an interesting component in electronics. TiO_2 exists in three different stable modifications and has good electrical, catalytic and electrochemical properties [9]. Literature has also shown that nanoscale TiO_2 reinforcement brings new optical, electrical, physiochemical properties attained at very low TiO_2 content, which make polymer TiO_2 nanocomposites a promising new class of materials. Among different inorganic nanofillers, TiO_2 was used to enhance some properties of polymer matrix [10]. Various methods have been used to produce titanium dioxide powders in the past two decades, such as the classic sulfate process, the chloride route, the sol–gel method [11, 12], the hydrothermal method [13–15] and the gas condensation method [16, 17]. The sol–gel method has generated a large scope of interest in the preparation of inorganic ceramic and glass materials. This simple, cost effective and low temperature synthesis procedure has also been favored and largely applied in catalyst preparation due to its potential to fabricate catalysts with high purity, homogeneity, fine-scale and controllable morphology.

Epoxy resins are thermosetting materials that require a cure treatment to attain suitable physical, optical, electrical and mechanical properties for industrial applications. Neat epoxy and epoxy reinforced nanoparticles are preferred chemicals, electrically insulating and adhesive materials for several applications, such as printed circuit boards, bushings, generator ground wall insulation systems and cast resin transformers. Excellent adhesive properties, resistance to heat and chemicals and very good electrical insulating properties make epoxy a favoured insulating material [18]. Bauer et al. [19] showed that a high content of nanosized silica, alumina, and Titania was embedded in epoxy adhesives. Yang et al. [20] proved a UV/IR blocking in the neat epoxy via the addition of inorganic nanoparticles. Chau et al. [21] show that the obtained refractive index of adding 30 wt% TiO_2 nanoparticles into the epoxy matrix via sol–gel method was found to be 1.668. Recently, compared to neat epoxy and epoxy with nanoparticles content, epoxy nanocomposites systems have displayed enhanced electric and optical properties [22]. Fujishima et al. [23] found that the TiO_2 possesses strong photocatalytic properties and excellent ultraviolet absorption properties which are effective for aging-resistant properties of polymers. Morselli et al. [24] were synthesized by means of TiO_2 generated nonhydrolytic sol–gel process mixed with a cycloaliphatic epoxy resin. It found that the presence of Titania nanoparticles resulted in a reinforcing and stiffening effect due to both their hydrodynamic effect and, most important, a significantly higher cross-linking density of the composite material with respect to the unfilled epoxy resin. The solid content of Titania in the epoxy matrix can be more than 70 wt% without affecting the optical transparency of the hybrid film [25]. Sowntharya et al. [26] synthesized hybrid nanocomposite coatings from titanium tetraisopropoxide, and epoxy or acrylic modified silanes were deposited on polycarbonate.

This article focuses to study the TiO_2 filler effect on microstructure and opto-electrical properties of Epoxy–TiO_2 composites (Ep–TiO_2–Cs). The band gap energy of Ep–TiO_2–Cs was determined and its comparison with the other data published in the literature was also studied. In addition, the important optical parameters of this study such as real and imaginary dielectric constants, optical conductivity, electric conductivity and VELF and SELF were also evaluated.

2 Experimental Techniques

2.1 Synthesis of the As-Prepared TiO_2 Particles

The TiO_2 powder is prepared by using sol–gel method [27]. We dissolved 5.5 ml of Titanium (IV) isopropoxide in 18 ml of methanol under magnetic stirring for 1.5 h and then we added 1.3 ml of acetic acid under magnetic stirring for 1 h. Finally, TiO_2 particles were obtained after calcination in an oven at 300 °C for 3 h.

2.2 Synthesis of Epoxy–TiO_2-Composites

The 2,2-bis (4-glycidyloxyphenyl) propane epoxy resin (molar mass 340 g/mol), and difunctional amine hardener provided by Maestria, are used to prepare the polymeric matrix. The epoxy resin and hardener are used in a molar ratio (75:25). Epoxy–TiO_2-composites (Ep–TiO_2–Cs) were synthesized using the ultrasonication mixing method to disperse TiO_2 fillers in epoxy matrix as described in previous work [22]. The obtained Ep–TiO_2–Cs samples, with 0.1; 0.2; 0.5; 1.0; 3.0 and 5.0 wt% TiO_2 contents, have thicknesses about 1.19 mm.

2.3 Characterization Techniques

Scanning electron microscopy (SEM) operating at 15 kV was used to get the morphological information of TiO_2 fillers and Ep–TiO_2–Cs systems.

The synthesized as prepared TiO_2 particles, neat epoxy and Ep–TiO_2–Cs samples were studied using X-Ray diffractometer (XRD) (Shimadzu LabX XRD-6000) of monochromatic Cu Kα radiation source operating at 40 kV voltage and 30 mA current. We used a step of 0.02° per second in the angular range of 10°–70° to confirm the "crystallinity" of the composite samples. Afterthought, crystallite size, dislocation density and lattice strain were determined.

The absorbance $A(\lambda)$, transmittance $T(\lambda)$ of the Ep–TiO_2–Cs samples, over the wavelength range of 200–1000 nm, were investigated using UV–Vis–NIR spectrophotometer (Shimadzu UV-3101). The absorption coefficient (α), the band gap energy (E_g), the extinction coefficient (k), the real and imaginary permittivity parts (ε_1, ε_2), the refractive index (n), the surface and volume energy loss functions (SELF, VELF) are calculated from the recorded data.

3 Results and Discussions

3.1 Surface Morphology of Ep–TiO_2–Cs Samples

The SEM was also done for the neat resin and its composite samples. The typical microstructure of the as prepared TiO_2 particles, neat epoxy and 5.0 wt% TiO_2 contents into epoxy resin were shown in Fig. 1. As shown in Fig. 1a, a separate particle can be distinguished. It exhibits that TiO_2 particles are spherical in shape. The obtained medium diameter of the synthesized as prepared TiO_2 particles is 4.23 µm. The fracture surface of the neat epoxy reveals a brittle behavior characterized by large smooth area and flat surface due to any reinforcing action which corresponds to the low growth of crack like defects (see Fig. 1b). As it can be seen in From Fig. 1c, it is found that a suitable adhesion between TiO_2 spheres content and the resin matrix have been attained at high level of loading 5.0 wt% TiO_2 composite samples. Furthermore, the micrograph exhibits a rough surface morphology and TiO_2 spheres can be identified on the surface of epoxy with 5.0 wt% TiO_2 composite sample. The overall size distribution of TiO_2 spheres is observed to be narrow and the overall dispersion of particles within the epoxy matrix is quite uniform. It seems that the cohesion of

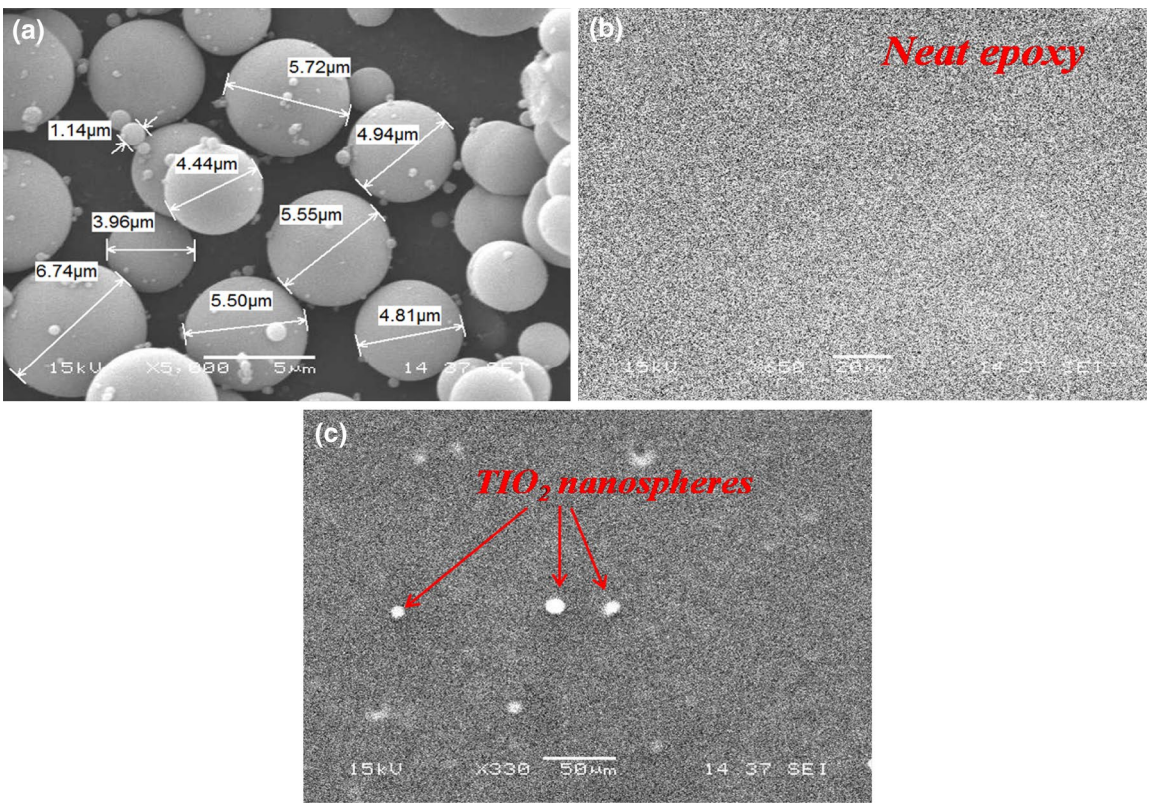

Fig. 1 SEM representative images of **a** the TiO_2 nanospheres, **b** the neat epoxy and **c** 5.0 wt% TiO_2 in epoxy resin

the TiO_2 spheres fillers and the viscosity of the resin might prevent the uniform dispersion. Furthermore, TiO_2 spheres seem to be well embedded into the matrix showing excellent particles–matrix adhesive, which may be attributed to weak physical interactions of TiO_2 spheres and epoxy matrix. The morphologies of fractured surface show brittle fracture with dispersed stresses in more than one crack propagation direction and less flat area with existence of TiO_2 sphere particles.

3.2 XRD Analysis of Ep–TiO_2–Cs Samples

XRD is the best tool to characterize the structure of the as prepared TiO_2 particles, neat epoxy and Ep–TiO_2–Cs to investigate the effect of TiO_2 spheres on the epoxy matrix. Figure 2 presents the typical XRD patterns of as prepared TiO_2 particles, neat epoxy, and Ep–TiO_2–Cs. The as prepared TiO_2 particles were confirmed to be a tetragonal structure with space group $I4_1/amd$. The deduced lattice parameters are found to be $a = 3.7852$ Å and $c = 9.5139$ Å, matching with data from JCPDS card No: 21-1272. The as prepared TiO_2 particles synthesized by sol gel method acquired enhanced structure. The XRD patterns of the Ep–TiO_2–Cs (in the contents of 1.0, 3.0 and 5.0 wt% TiO_2 contents) show dominant peak with values of 2θ located at 25.28°, 37.8°, 48.04°, 53.5°, 53.89° and 62.68°, corresponding to the (101), (004), (200), (105), (211) and (204) indexed planes, respectively. They indicate that the added TiO_2 fillers have the crystal phase of anatase. The strong and sharp diffraction peaks showed highly crystalline TiO_2 contents. From Fig. 2, it is evident that neat epoxy and the composites systems exhibit a broad diffraction peak at approximately $2\theta = 19°$ which reveals the amorphous nature of the Epoxy matrix [8]. The small diffraction peak in the (0.1, 0.2 and 0.5 wt% TiO_2 samples) indicates that the low TiO_2 content was uniformly dispersed into epoxy matrix and it is also a strong evidence for the formation of an exfoliated composite structure. Incorporated and confined TiO_2 particles into epoxy matrix (at 3.0 and 5.0 wt% TiO_2) through the curing process of composites showed a significant diffraction peaks relative to TiO_2 anatase.

To estimate the better orientation of crystal planes of TiO_2 confined structure in Epoxy matrix, the texture coefficient $T_{C(hkl)}$ was determined using the following equation [28].

$$T_{C(hkl)} = \frac{I_{(hkl)}}{I_{0(hkl)}} \Big/ \frac{1}{n} \sum_i \frac{I_{(hkl)i}}{I_{0(hkl)i}}, \tag{1}$$

where $I_{(hkl)}$ is the measured intensity of the (hkl) X-ray reflection, $I_{0(hkl)}$ is the corresponding intensity for randomly oriented sample taken from the JCPDS card No: 21-1272 and 'n' is the number of diffraction peaks observed in the XRD patterns. The variation of T_C with the crystal planes peaks for TiO_2 in all Ep–TiO_2–Cs samples is shown in Fig. 3. As shown in this figure, the similar deviation among the $T_{C(hkl)}$ of various facets (hkl) is observed for different added TiO_2 fillers in an epoxy matrix. It can be easily remarked that no preferential orientation of TiO_2 particles is observed. Using Scherer's equation, the particle size of the added TiO_2 contents is evaluated [29]:

$$D = \frac{0.9\lambda}{\beta cos\theta}, \tag{2}$$

where D is the particle size of the added fillers in the epoxy matrix, λ is the wavelength ($\lambda = 1.5418$ Å), β is the full width at half maximum and θ is the scattering Bragg angle. The

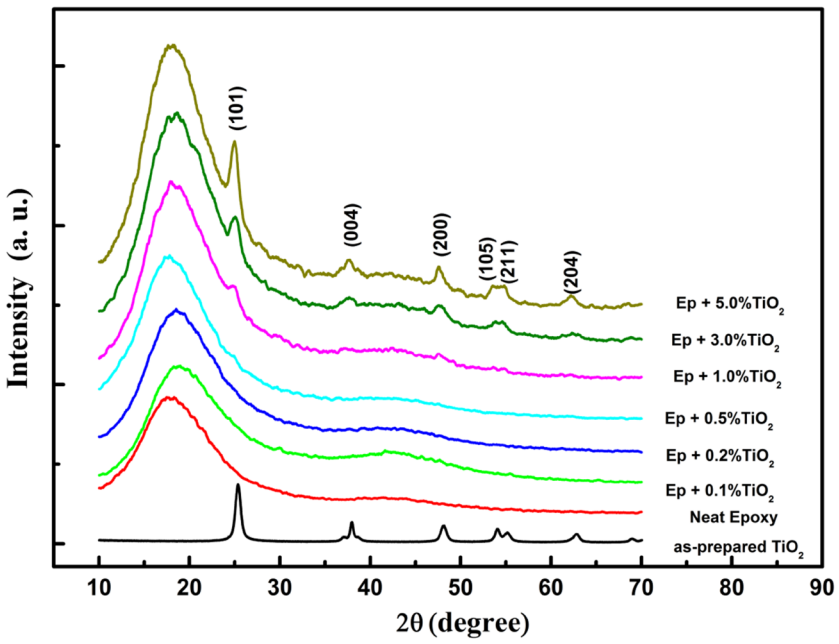

Fig. 2 XRD patterns of TiO_2 nanospheres and Ep–TiO_2–NCs with different content of TiO_2

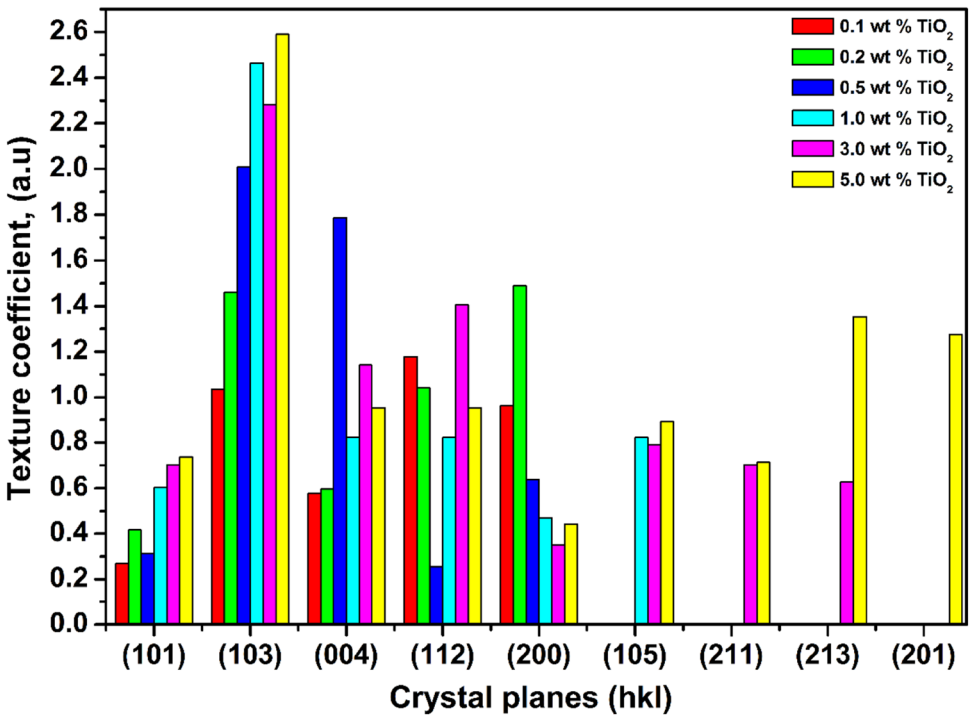

Fig. 3 Texture coefficient upon (*hkl*) crystal planes for Ep–TiO_2–NCs

obtained values of 2θ and FWHM are gathered and added in Table 1.

The internal strain of TiO_2 in the composite systems is calculated using the formula [30]:

$$\varepsilon = \frac{\beta cos\theta}{4}, \tag{3}$$

Also, the dislocation density (δ) is established using the relation [30]:

$$\delta = \frac{1}{D^2}, \tag{4}$$

The particle size (D), dislocation (δ) and internal strain (ε) analysis results of TiO_2 nanoparticles embedded in the Ep–TiO_2–Cs are given in Fig. 4. From Fig. 4, we can easily note that the average size of TiO_2 particles embedded in the epoxy matrix decreases with increasing the added TiO_2 fillers. The average size decreases from about 50 nm in 1.0 and 3.0 wt% TiO_2 to 30 nm in 5.0 wt% TiO_2 sample, indicating the better dispersion of TiO_2 particles in highly filled epoxy matrix. Also, the dislocation and the internal strain increase with increasing added TiO_2 contents, in agreement with the particle size decrease, which can provide the information about the good dispersion of TiO_2 particles in the epoxy matrix. This confirmed the observed SEM representative micrograph of Ep–TiO_2–Cs with 5.0 wt% TiO_2 contents (Fig. 1).

Table 1 The values of peak position 2θ and FWHM for TiO_2/epoxy composites

0.1 wt% TiO_2		0.2 wt% TiO_2		0.5 wt% TiO_2		1.0 wt% TiO_2		3.0 wt% TiO_2		5.0 wt% TiO_2	
2θ	θ	2θ	FWHM	2θ	FWHM	2θ	FWHM	2θ	FWHM	2θ	FWHM
25.43	0.146	24.592	0.125	24.93	0.413	25.02	0.68	25.05	1.07	24.98	0.875
36.63	0.31	37.886	0.052	36.6	0.08	37.07	0.3	37.16	0.18	36.81	0.113
48.17	0.141	48.26	0.08	38.87	0.18	37.96	0.24	37.6	0.66	37.5	0.5
53.52	0.17	54.93	0.06	47.47	0.14	38.9	0.03	38.2	0.32	38.69	0.22
63.09	0.19	62.56	0.18	62.33	0.19	47.9	0.15	48.24	0.04	48.02	0.16
						53.57	0.22	53.84	0.64	53.46	0.306
								54.9	0.2	54.82	0.52
								63.06	0.31	62.14	0.64
										62.48	0.48

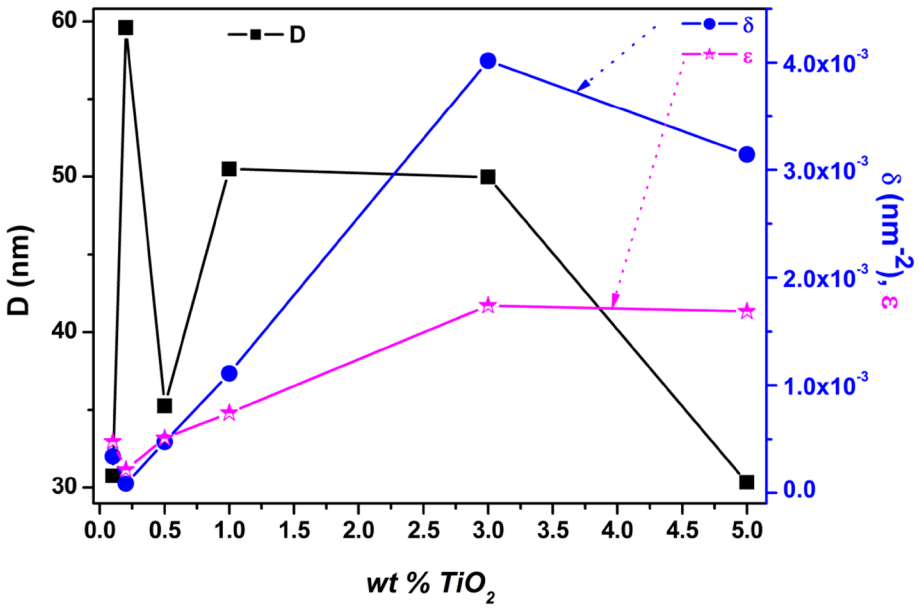

Fig. 4 Evolution of crystallite size (D), dislocation (δ) and internal strain (ε) analysis for different incorporating TiO_2 nanospheres

3.3 Linear Optical Properties of Ep–TiO_2–Cs Samples

The effect of TiO_2 spheres fillers on the linear optical properties of Ep–TiO_2–Cs has been probed using UV–Vis–NIR spectrophotometer. Optical characterization like transmittance, absorbance, absorption coefficient, refractive index and energy band gap provide basic information about the quality and gives electrical properties of the prepared materials. Figure 5 shows the variation of transmittance and absorbance spectra of the Ep–TiO_2–Cs with different TiO_2 contents, recorded in the wavelength range of 200–1000 nm. From As it can be seen in Fig. 5a, the transmittance of the neat epoxy is high in the visible and NIR range. The neat epoxy system exhibits an excellent transparency of more than 60% of the visible light, and reaches 80% in the NIR range. Whereas Ep–TiO_2–Cs transmittance falls to less than 10% when the TiO_2 contents into epoxy matrix increases up to 5.0 wt% TiO_2. This transmittance shrinkage is more important in the NIR range for the highly-filled composites (see the inset of Fig. 5a). Therefore, adding TiO_2 contents in epoxy matrix obviously improves the UV-shielding efficiency, with an enhancement of about 65–80% up to 5.0 wt% TiO_2.

An alternative cause of light scattering is the mismatch of refractive index between the polymer matrix and the particles (the refractive index of epoxy polymer is 1.54–1.55 [31], and that of TiO_2 is 2.6–2.9 [32, 33]) which leads to intense light scattering [34]. In the same way, the intensity losses of incident light can be described by [35, 36]:

$$\frac{I}{I_0} = \exp[\frac{-3V_p\chi\, r^3}{4\lambda^4}(\frac{n_p}{n_m} - 1)], \quad (5)$$

where r is the radius of valued spherical particles, n_p and n_m are the refractive indices of the particles and the matrix respectively, I is the intensity of the scattered light, I_o the intensity of incoming light for non-absorbing materials, V_p is the volume fraction of the particles, λ is the light wavelength and is the optical path length. The above equation indicates that in the presence of mismatching of refractive index, the scattered light intensity decreases with increasing the particle radius r. Thus, the RI incompatibility may be compensated by the reduction of the particle size under visible light wavelength, and therefore transparency can be kept at a level relatively high. But if the particle size grows, the particle agglomeration becomes important. These agglomerations persist in the composites and scatter visible light.

Besides, in the UV-light region, the transmittance drops sharply due to the onset of fundamental absorption. Furthermore, the UV-light absorption was extended up to about 400 nm for the 5.0 wt% TiO_2 filled composites (Fig. 5b). Figure 5b shows the changes in the absorbance spectra of neat epoxy and Ep–TiO_2–Cs. The Ep–TiO_2–Cs samples were found to have higher visible absorbance in comparison to neat epoxy. It is important to mention that the absorption edge of composite samples, instead of being abrupt, occurs quite smoothly. The transmittance of sample 5.0 wt% TiO_2 nearly reached zero at the range of 200–280 nm (see Fig. 5a), indicating that the TiO_2 spheres fillers in epoxy matrix possessed a strong UV absorbance, which was also confirmed in other papers [37]. In the UV-light range, the neat epoxy polymer only blocks UV-light in the range of 200–280 nm, however it becomes high UV-light blocker (up to 400 nm) via the addition of TiO_2 powder from 5.0 wt% filling concentration. These results prove that the Ep–TiO_2–Cs can be potential candidates to be used in the UV-shielding coatings.

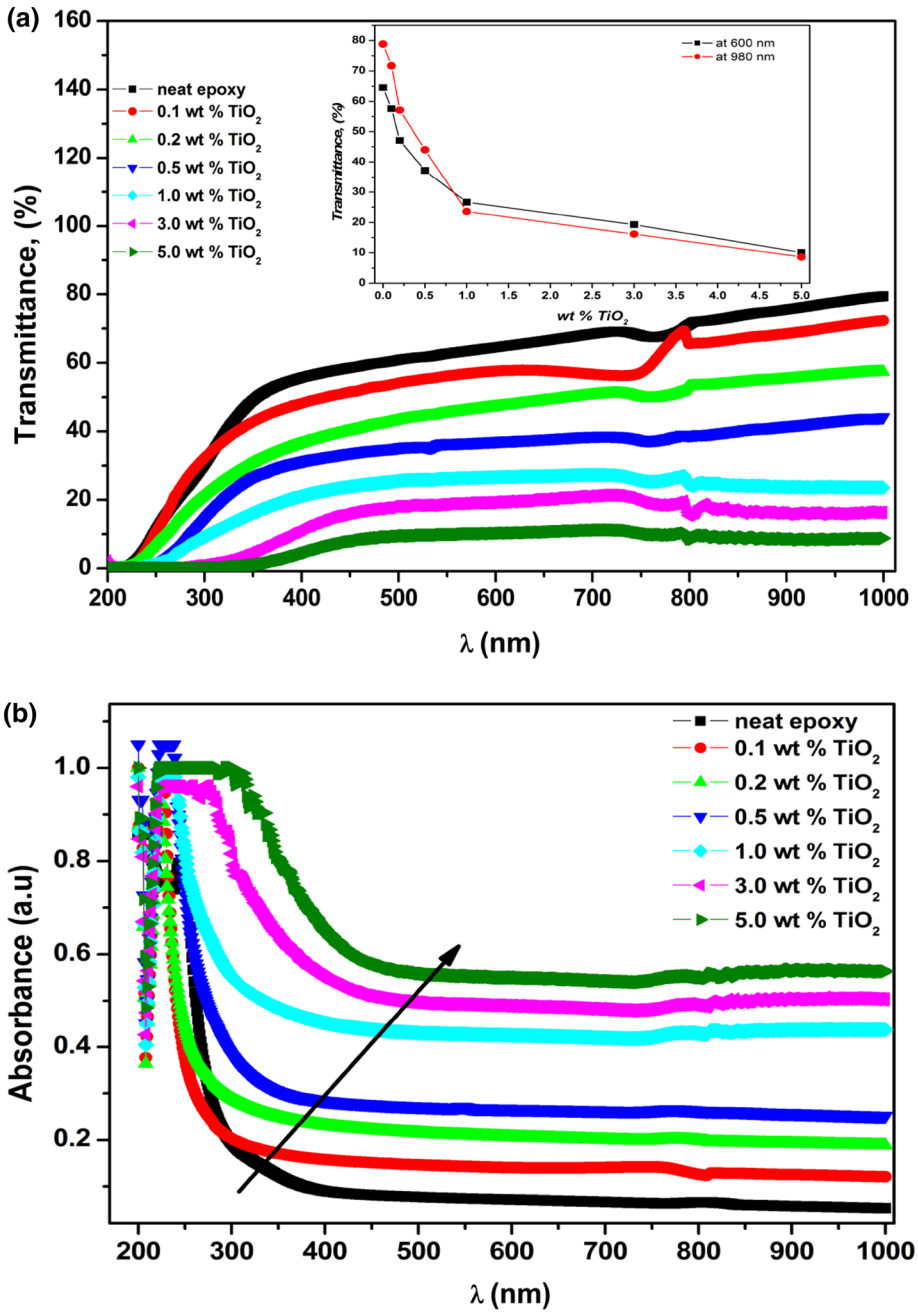

Fig. 5 Variation of **a** transmittance and **b** absorbance upon wavelength of Ep–TiO_2–NCs

Using Tauc's model, the optical band gap energy (E_g) of synthesized Ep–TiO_2–Cs was calculated from the absorption data [38, 39]:

$$(\alpha h\upsilon)^m = A(h\upsilon - E_g) \tag{6}$$

where A is the pre-factor constant independent of photon energy for this transition, in this case, $m=2$ is a parameter if the band transition is direct, and $h\nu$ is the incident photon energy. α is the absorption coefficient evaluated from absorbance data. The calculated values of $(\alpha h\nu)^2$ versus $(h\nu)$ are plotted in Fig. 6a. The band gap energies are obtained by extrapolating the linear portion of the graph on the hν axis at $(\alpha h\nu)^2 = 0$, as shown in Fig. 6a.

The obtained values of direct gap energy E_g are plotted in Fig. 6b as a function of TiO_2 content. It is clear that the band gap decreases with increasing TiO_2 contents in epoxy matrix, which reflects the change in the electronic structure of the epoxy matrix. This decrease is due to the interactions between TiO_2 particles and epoxy matrix. In addition, the decrease in optical band gap can be related to the increasing in the density of defect states [40, 41]. Indeed, polymer

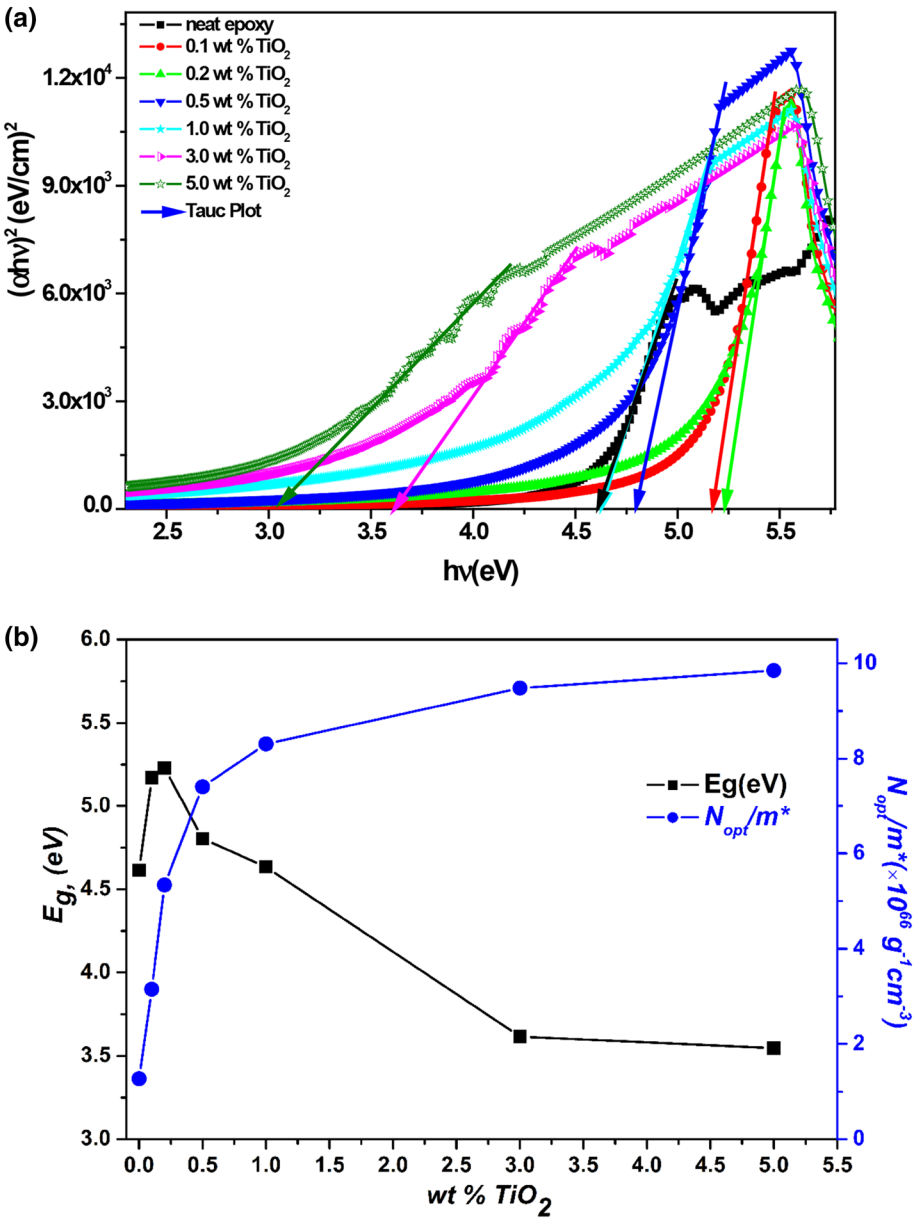

Fig. 6 **a** Tauc's plots of variation of optical band gap and **b** variation of direct band gaps and constant *A* for our samples

composites contain a high concentration of defect states and these defects are responsible for the presence of localized states in the band gap. So, it can be explained by the broadening of the valance band inside the forbidden gap and leads to band tailing and hence band gap shrinkage.

Extinction coefficient (k) and refractive index (n) are often referred to as the optical constants of the material. Together, n and k have a key role to determine several optical properties of the composite. The refractive index (n) was determined from the transmittance spectrum as function of the wavelength in the range of 200–1000 nm. The value of n can be determined by using Fresnel relation based on the reflectance R and the extinction coefficient k is as follows [22]:

$$n = \frac{1+R}{1-R}\sqrt{\left(\frac{4R}{(1-R)^2} - k^2\right)}, \tag{7}$$

where, $k = \alpha\lambda/4\pi$ is the extinction coefficient. Those optical parameters were shown in Fig. 7 for Ep–TiO_2–Cs systems. The extinction coefficient is inversely related to the transmittance spectra. From Fig. 7a, it is found that the value of extinction coefficient k is larger which proved that there is a strong absorption at 5.0 wt% TiO_2 sample compared to the neat epoxy. The value of k generally varying with added TiO_2 contents and shows that the neat epoxy is highly transparent. The extinction coefficient was found to be high. The values indicate the loss of electromagnetic radiation energy

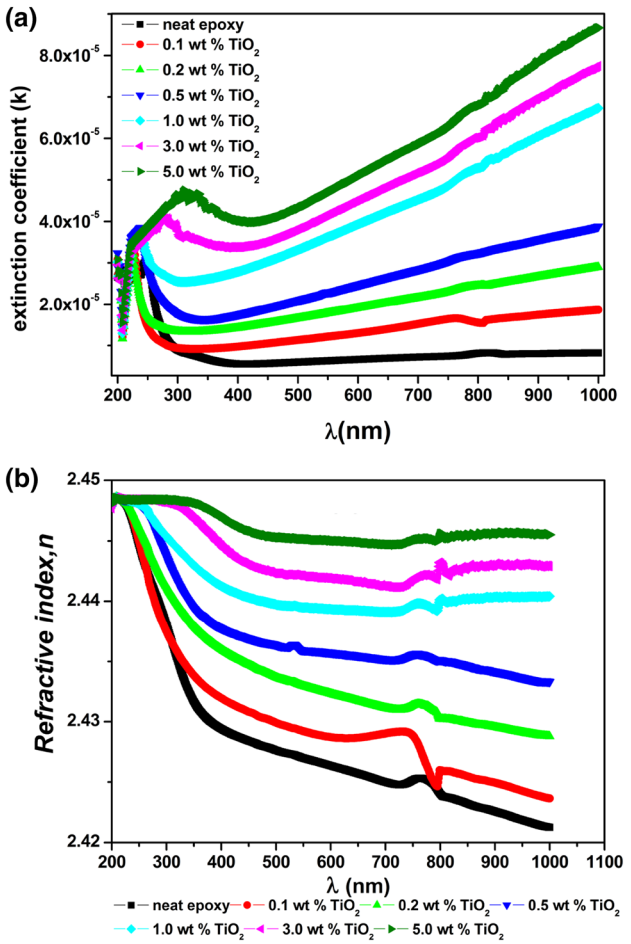

Fig. 7 **a** Variation of extinction coefficient and **b** dependence of the refractive index upon to wavelength for different TiO_2 nanospheres content

through medium of the material. It is clear that the *k* values are slighter at the lower wavelengths and exceedingly important at high frequencies. At the high added TiO_2 contents, it is highly transparent compared to the neat epoxy sample. The variation in the *k* values is may attribute to the light scattering resulting from the interface between the increasing added nanoparticles into the epoxy matrix.

The refractive index *n* is an important physical parameter related to microscopic atomic interactions. Figure 7b represented the variation of the refractive index n for Ep–TiO_2–Cs upon the wavelength. As shown in this figure, the increase in added TiO_2 fillers results in overall increasing of the refractive index which due to the largely decreasing of transmission as TiO_2 content in epoxy matrix increases. It is used to achieve both electronic polarization and the applied electric local field inside the optical materials. In UV–Vis region, the refractive index becomes constant in the higher added TiO_2 contents at the content 3.0 and 5.0 wt%. Also, the refractive index values were remaining almost unchanged with added TiO_2 contents. It is found to be 2.448 at a high content of TiO_2 concentrations, which resulting in higher reflection; the highest value of refractive index is suitable for optical devices.

The dielectric function is a complex quantity and a fundamental intrinsic property of the composite material which consists of both real and imaginary parts. The real part indicates how the speed of light in the material can be slowed down due to the scattering effect at the material grains and boundaries and it is related to *n* value. While, the imaginary part deals with the energy absorption from electric field due to dipole motion and it is related to *k* value. Using the complex dielectric permittivity ε^*, we can be determined other optical parameters such as the volume and surface energy loss functions (VELF) and (SELF) of the solid material, respectively and relaxation time τ. It can be calculated from the relation:

$$\varepsilon^* = \varepsilon_1 + i\varepsilon_2, \tag{8}$$

With values of refractive index *n* and extinction coefficient *k*, we can be deduced the real and imaginary parts of the dielectric permittivities ε_1 and ε_2 for Ep–TiO_2–Cs using the following equations [42]:

$$\varepsilon_1 = n^2 - k^2, \tag{9}$$

$$\varepsilon_2 = 2nk, \tag{10}$$

From Eqs. (7 & 8), several optical constants can be determined such as the dielectric permittivity at high frequencies ε_∞, the plasma frequency ω_p and relaxation time τ, about the relations [43]:

$$\varepsilon_1 \approx \varepsilon_\infty - \frac{\varepsilon_\infty \omega_p^2}{4\pi^2 c^2}\lambda^2, \tag{11}$$

$$\varepsilon_2 = \frac{\varepsilon_\infty \omega_p^2}{8\pi^3 c^3 \tau}\lambda^3, \tag{12}$$

The intrinsic carrier's concentration related to the effective mass ratio N_{opt}/m^* is then calculated using:

$$\omega_p^2 = \frac{4\pi N_{opt} e^2}{\varepsilon_\infty m_e^*}, \tag{13}$$

At high electromagnetic waves, it is considered that the real part ε_1 of the dielectric permittivity was related to the dispersion energy of the propagation speed through the material. However, the imaginary part ε_2 of the dielectric permittivity was responsible for the energy absorption from the applied electric field due to dipole motion [44]. For all samples and in the IR range, it is found that the real part of the dielectric permittivity has a linear portion in

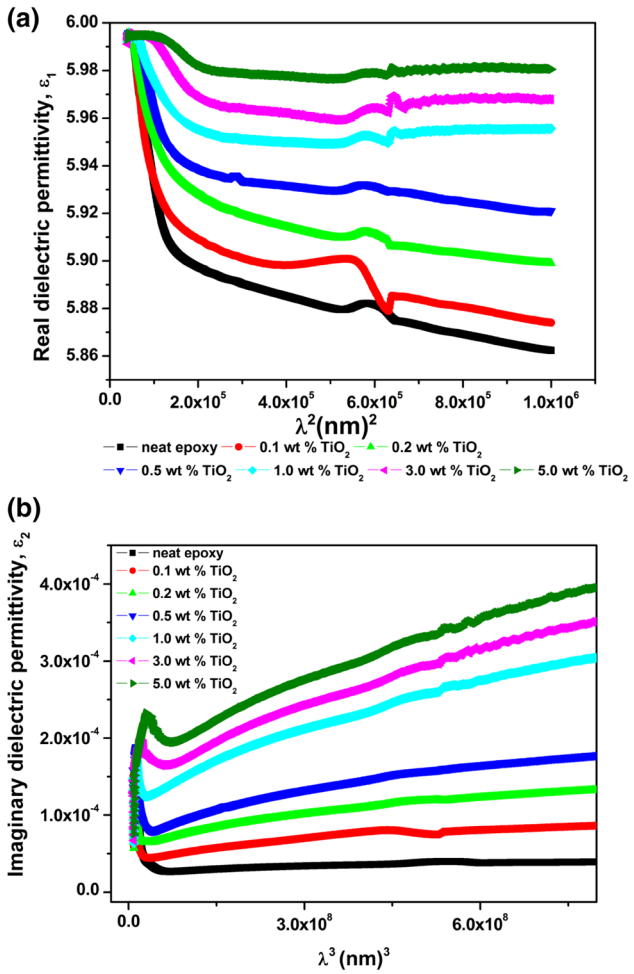

Fig. 8 **a** Real part of dielectric permittivity versus λ^2 and **b** Imaginary part of dielectric permittivity versus λ^3

the representative square of the wavelength (see Fig. 8a), meanwhile the imaginary part is linear with λ^3, as shown in Fig. 8b. The variation of the dielectric permittivity with the wavelength was occurred some molecular interactions between the TiO_2 contents and epoxy matrix through curing process. The calculated values of these dielectric permittivities have been gathered in Table 2. Using the Table 2, it is noted that all optical parameters were decreased linearly in composites system compared to neat epoxy when increasing the added TiO_2 fillers quantities in the epoxy matrix. To confirm the red shift of the band gap energy in Ep–TiO_2–Cs, the optical resistivity ρ_{opt} of the investigated Ep–TiO_2–Cs can be determined by using the values of N_{opt}/m^* and τ, from the equation [45]:

$$\rho_{opt} = \frac{m^*}{e^2 \tau N_{opt}} \tag{14}$$

The estimated values of optical resistivity for Ep–TiO_2–Cs were summarized in Table 1. The intrinsic carrier concentration N_{opt}/m^* in composite systems was calculated and then its variation with TiO_2 content was presented in Fig. 6b. It can be obviously noted that the red shift of band gap energy is related to the increase of carrier concentration in Ep–TiO_2–Cs. The variation of optical resistivity for differently prepared samples was illustrated in Fig. 9. From this figure, the optical resistivity decreased with increasing TiO_2 contents compared to neat epoxy. It is close to the good insulator system of the epoxy polymer.

The optical properties originated from movement of the electron inside the lattice optical conductivity. The optical conductivity directly depends on the absorption coefficient and refractive index of the material and follows the same trend as the absorption coefficient and refractive index with increasing wavelength. We used the absorption coefficient α to evaluate the optical and electrical conductivity σ_{opt} and σ_e respectively, and is shown in Fig. 10 as following relationships [46]:

$$\sigma_{opt} = \frac{\alpha n c}{4\pi}, \tag{15}$$

$$\sigma_e = \frac{2\lambda\sigma_{opt}}{\alpha}, \tag{16}$$

where c is the velocity of light. As can be shown in Fig. 10, the added TiO_2 fillers in epoxy matrix greatly increased the optical conductivity and the electric conductivity was increased at $\lambda = 700$ nm in the Ep–TiO_2–Cs samples (see

Table 2 Calculated values of optical constants

Samples	ε_∞	ω_p ($\times 10^{14}$ rad/s)	τ ($\times 10^{-14}$ s)	N_{opt}/m^* ($\times 10^{66} g^{-1} cm^{-3}$)	ρ_{opt} ($\times 10^{-16}$ Ω cm)
Neat epoxy	6.048	8.24	1.26×10^{-14}	2.27	13.65
0.1 wt% TiO_2	6.042	7.84	1.308×10^{-14}	3.15	9.48
0.2 wt% TiO_2	6.029	6.67	1.32×10^{-14}	5.34	5.54
0.5 wt% TiO_2	6.04	6.69	3.23×10^{-14}	7.41	1.63
1.0 wt% TiO_2	6.019	5.07	3.32×10^{-14}	8.31	1.41
3.0 wt% TiO_2	6.017	3.84	8.08×10^{-14}	9.48	0.509
5.0 wt% TiO_2	6.01	2.88	9.44×10^{-14}	9.85	0.421

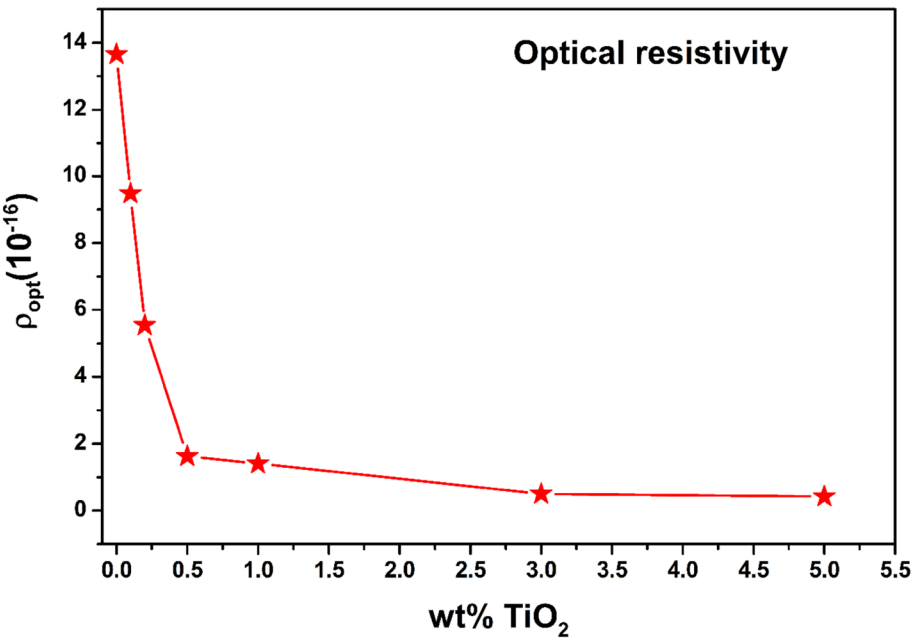

Fig. 9 Optical resistivity us function the added wt% TiO_2 nanospheres in epoxy matrix

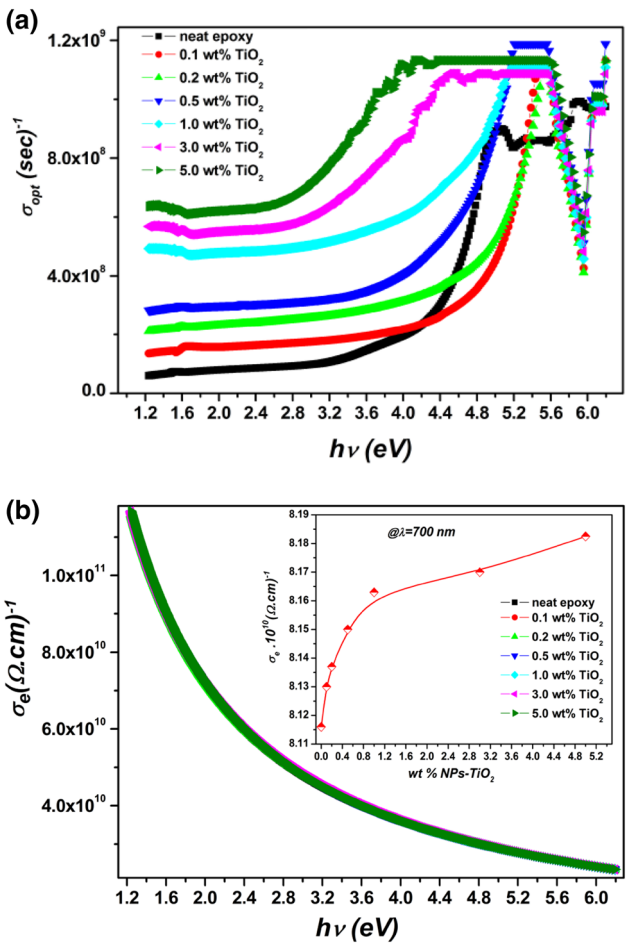

Fig. 10 **a** Optical conductivity and **b** electrical conductivity versus incident energy for different TiO_2 nanospheres content (the inset represents the evolution of σ_e us function of wt% TiO_2 nanospheres for $\lambda = 700$ nm)

inset Fig. 10b). The electrical conductivity of these composites has been affected by the presence of TiO_2 fillers content. The variation in optical conductivity with photon energy is related to the transmission for all prepared composite materials. The increase of optical conductivity in the high photon energy region is due to the high absorbance of the composite samples compared to neat epoxy and also may be due to the electron excited by photon energy, and with increasing adding TiO_2 content. This increase because of creation of new levels in the band gap, lead to facilitate the crossing of electrons from the valence band to these local levels to the conduction band, consequently the band gap decreases and the conductivity increase. As the results are agreements with other work [47].

The energy loss is related to the optical properties of the material through the dielectric function. The volume and the surface energy loss functions (*VELF and SELF*) can define the probability that the fast electrons will lose energy when migrant within the material and on its surface. These two functions are related to real and imaginary parts ε_1 and ε_2 of the complex dielectric constant by the following relationships [48]:

$$VELF = \frac{\varepsilon_2}{\varepsilon_1^2 + \varepsilon_2^2}, \tag{17}$$

$$SELF = \frac{\varepsilon_2}{(\varepsilon_1 + 1)^2 + \varepsilon_2^2}, \tag{18}$$

The variation of the volume and the surface energy losses as function wavelength of Ep–TiO_2–Cs were shown in Fig. 11. In the curves shown in Fig. 11a, it is revealed that

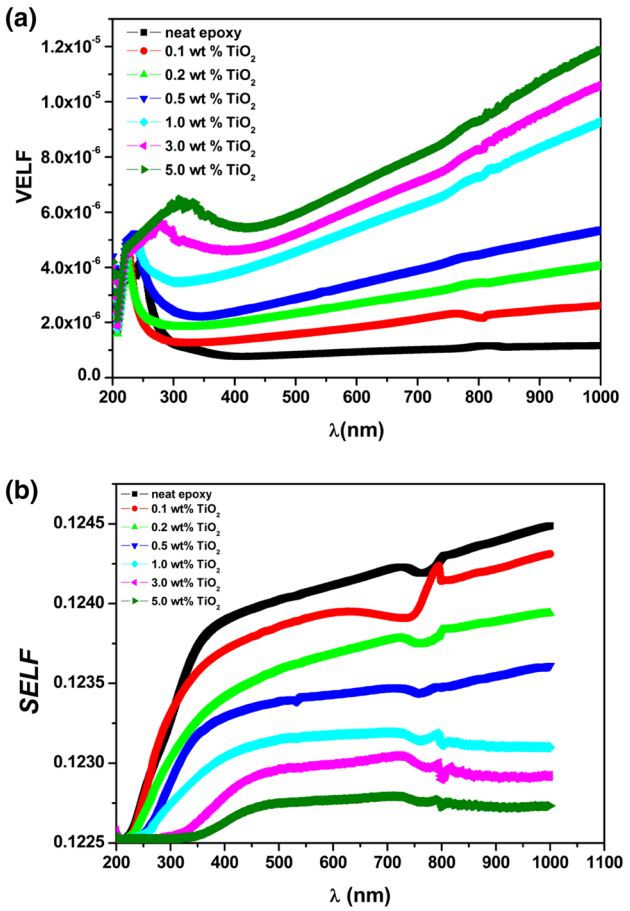

Fig. 11 **a** Evolution of the volume energy loss functions (VELF) and **b** surface energy loss functions (SELF) as function of wavelength of the Ep–TiO_2–NCs samples

the *VELF* curves increased with increasing TiO_2 contents and with increasing wavelength in visible and mainly in *NIR* region compared to neat epoxy. Up to 400 nm, the *VELF* values were strongly changed. This increased *VELF* with wavelength can be enabling these materials for electro-optical applications. In the other hand, the *SELF*-values decreased with added TiO_2 fillers quantities into the epoxy matrix (see Fig. 11b). The decreasing values of *SELF* lead to deduce that the materials improve the UV-shielding devices.

4 Conclusion

The TiO_2/epoxy composites (Ep–TiO_2–Cs) were prepared and characterized to investigate some advantageous optoelectronic behaviors at different TiO_2 contents compared to the neat epoxy. The obtained data from SEM analysis enhanced the homogenous and the uniform distribution of TiO_2 on the epoxy matrix. Furthermore, TiO_2 particles seem to be well embedded into the epoxy matrix. The data obtained from XRD analysis shows that grain size, dislocation, and strain were affected by the addition of TiO_2 contents. The experimental absorbance and transmittance data were investigated using the Ultra-Violet (*UV–Vis*) spectrophotometer. In the UV-light range, the neat epoxy polymer only blocks UV-light in the range of 200–280 nm, however it becomes high UV-light blocker (up to 400 nm) via the addition of TiO_2 nanopowder from 5.0 wt% filling concentration. The neat epoxy system exhibits an excellent transparency of more than 60% of the visible light, and reaches 80% in the *NIR* range. Whereas, Ep–TiO_2–Cs transmittance falls to less than 10% when the TiO_2 contents into epoxy matrix increases up to 5.0 wt% TiO_2. This transmittance shrinkage is more important in the *NIR* range for the highly-filled composites. The band gap decreases when the adding TiO_2 increases. This decreases due to the decrease of particle size. This property is called as red shift in the prepared composites. Optical parameters of composite samples are determined. Up to 400 nm, the *VELF* values were strongly changed. The *SELF* values decreased with added TiO_2 fillers quantities into the epoxy matrix. All optical parameters and dielectric studies of the investigated Ep–TiO_2–Cs samples prove that these composites are more suitable in their great potential of optoelectronic devices and UV-shielding coatings.

Acknowledgements This study has been supported by the Tunisian Ministry of High Education Scientific Research and Information and Communication Technologies, Tunisia (*ICTP through TWAS Grant No. 00-043 RG/PHYS/AF/AC*), Higher Education and Scientific Research sector. The authors also are grateful to the Research Center for Advanced Material Science (*RCAMS*) at King Khalid University, with grant number (*RCAMS-1-17-5*).

References

1. J.L.H. Chau, C.-T. Tung, Y.-M. Lin, A.-K. Li, Mater. Lett. **62**, 3416–3418 (2008)
2. T.L. Wang, C.C. Yu, C.H. Yang, Y.T. Shieh, Y.Z. Tsai, N.F. Wang, J. Nanomater. **2011**, 1–9 (2011)
3. M.Z. Rong, M.Q. Zhang, Y.X. Zheng, H.M. Zeng, R. Walter, K. Friedrich, J. Mater. Sci. Lett. **19**, 1159 (2000)
4. C. Becker, H. Krug, H. Schmidt, Mater. Res. Soc. Symp. Proc. **435**, 237 (1996)
5. G. Carotenuto, L. Nicolais, X. Kuang, Z. Zhu, Appl. Comp. Mater. **2**, 385 (1995)
6. Y. Duan, J. Liu, L. Ma, N. Li, H. Liu, J. Wang, L. Zheng, C. Liu, X. Wang, X. Zhao, J. Yan, S. Wang, H. Wang, X. Zhang, F. Hong, Biomaterials **31**, 894–899 (2010)
7. X. Chang, Y. Xie, J. Wu, M. Tang, B. Wang, J. Nanosci. Nanotechnol. **15**(2), 1135–1142 (2015)
8. P. Tao, Yu Li, A. Rungta, A. Viswanath, J. Gao, B.C. Benicewicz, R.W. Siegel, L.S. Schadler, J. Mater. Chem. **21**, 18623 (2011)
9. A. Welte, C. Waldauf, C. Brabec, P.J. Wellmann, Thin Solid Films **516**, 7256–7259 (2008)
10. A. Chatterjee, M.S. Islam, Mater. Sci. Eng. A **487**, 574–585 (2008)

11. M. Schneider, A. Baiker, J. Mater. Chem. **2**, 587 (1992)
12. B.E. Yoldas, J. Mater. Sci. **21**, 1087 (1986)
13. H. Cheng, J. Ma, Z. Zhao, L. Qi, Chem. Mater. **7**, 663 (1995)
14. C.C. Wang, J.Y. Ying, Chem. Mater. **11**, 3113 (1999)
15. S.T. Aruna, S. Tirosh, A. Zaban, J. Mater. Chem. **10**, 2388 (2000)
16. L. Shi, C. Li, A.P. Chen, Y.H. Zhu, D.Y. Fang, Mater. Chem. Phys. **66**, 51 (2000)
17. J. Rubio, J.L. Oteo, M. Villegas, P. Duran, J. Mater. Sci. **32**, 643 (1997)
18. D. Rosu, C.N. Cascaval, F. Mustata, C. Ciobanu, Thermochim. Acta **283**, 119–127 (2002)
19. F. Bauer, U. Decker, H. Ernst, M. Findeisenb, H. Langguth, R. Mehnert, V. Sauerland, R. Hinterwaldner, Int. J. Adhes. Adhes. **26**, 567 (2006)
20. Y. Yang, Y.Q. Li, S.Y. Fu, H.M. Xiao, J. Phys. Chem. C **112**, 10553–10558 (2008)
21. Z. Rubab, A. Afzal, H.M. Siddiqi, S. Saeed, Sci. World J. **2014**, 1–8 (2014)
22. A. Bouzidi, K. Omri, L. El Mir, H. Guermazi, Mater. Sci. Semicond. Process. **39**, 536–543 (2015)
23. A. Fujishima, T.N. Rao, D.A. Tryk., J. Photochem. Photobiol. C **1**, 1 (2000)
24. D. Morselli, F. Bondioli, M. Sangermano, I. Roppolo, M. Messori, J. Appl. Polym. Sci. (2014). https://doi.org/10.1002/APP.40470
25. J.L.H. Chau, H.W. Liu, W.F. Su, J. Phys. Chem. Solids **70**, 1385 (2009)
26. L. Sowntharya, S. Lavanya, G. Ravi Chandra, N.Y. Hebalkar, R. Subasri, Ceram. Int. **38**, 4221 (2012)
27. K. Omri, I. Najeh, L. El Mir, Ceram. Int. **42**, 8940–8948 (2016)
28. S. Kumar, S. Kumar, P. Sharma, V. Sharma, S.C. Katyal, J. Appl. Phys. **112**, 1–8 (2012)
29. R. Chauhan, A.K. Srivastava, A. Tripathi, K.K. Srivastava, Prog. Nat. Sci. **21**, 205 – 210 (2011)
30. C.C. Wang, Phys. Rev. B **2**, 2045 (1970)
31. D.Y.S. Luo, J.P. Yang, X.J. Dai, Y. Yang, S.Y. Fu, J. Phys. Chem. **C113**, 9406 (2009)
32. R.J. Nussbaumer, W.R. Caseri, P. Smith, T. Tervoort, Macromol. Mater. Eng. **288**, 44–49 (2003)
33. D.R. Lide, *Handbook of Chemistry and Physics*, 76th edn. (CRC Press, Boca Raton, 1995)
34. J. Ederth, P. Johnsson, G. Niklasson, A. Hoel, A. Hultaker, P. Heszler, C. Granqvist, A.R. .Doorn, M. Jongerius, D. Burgard, Phys. Rev. **B68**, 155410 (2003)
35. Y.S. Luo, J.P. Yang, X.J. Dai, Y. Yang, S.Y. Fu, J. Phys. Chem. C **113**, 9406 (2009)
36. H.C. Huang, T.E. Hsieh, Ceram. Int. **36**, 1245 (2010)
37. J.J. Tang, C.H. Su, J. Jiangsu Univ. Sci. Technol. Nat. Sci. Ed. **23**, 125 (2009)
38. S.Hong,E. Kim, D.-W. Kim, T.-H. Sung, K. No, J. Non-Cryst. Solids **221**, 245–254 (1997)
39. P. Singh, A. Kaushal, D. Kaur, J. Alloy. Compd. **471**, 11–15 (2009)
40. N.F. Mott, E.A. Davis, *Electronic Processes in Non-Crystalline Materials*, (Clarendon, Oxford, 1979) p. 428
41. K. Sharma, M. Lal, A. kumar, N. Goyal, J. Optoelect. Biomed. Mater. **6**, 19 (2014)
42. M.A. Omar, *Elementary Solid State Physics*, (Addison-Wesley Publishing Company, New York, 1993)
43. M. Sesha Reddy, K.T. Rama Krishna Reddy, B.S. Naidu, P.J. Reddy, Opt. Mater. **4**, 787–790 (1995)
44. Q. Shen, K. Katayama, T. Sawada, T. Toyoda, Thin Solid Films **516**, 5927–5930 (2008)
45. F. Lai, L. Lin, R. Gai, Y. Lin, Z. Huang, Thin Solid Films **515**, 7387–7392 (2007)
46. J.I. Gittleman, E.K. Sichel, Y. Arie, Solar Energy Mater. **1**, 93–104 (1979)
47. M.M. El-Desoky, I.M. Morad, M.H. Wasfy, A.F. Mansour, IOSR J. Appl. Phys. **9**, 33–43 (2017)
48. S. Sarkar, N.S. Das, K.K. Chattopadhyay, Solid State Sci. **33**, 58–66 (2014)